Design of Attitude Control Systems for CubeSat-Class Nanosatellite

Article *in* Journal of Control Science and Engineering · May 2013

DOI: 10.1155/2013/657182

4 authors, including:

Mark Post
University of Strathclyde
21 PUBLICATIONS **54** CITATIONS
SEE PROFILE

Regina Lee
York University
26 PUBLICATIONS **65** CITATIONS
SEE PROFILE

Design of Attitude Control Systems for CubeSat-Class Nanosatellite

Junquan Li*, Mark Post, Thomas Wright, Regina Lee
junquanl@yorku.ca, *markpost@yorku.ca*, *tjlayer@yorku.ca*, *reginal@yorku.ca*

York University, 4700 Keele Street, Toronto, ON, M3J 1P3, Canada

Abstract

Low cost hardware and software for a 1U CubeSat with an active attitude control subsystem is presented in this paper. The Attitude Control System (ACS) architecture is a crucial subsystem for any satellite mission since precise pointing is required to meet mission objectives. The accuracy and precision requirements are even more challenging for small spacecraft where limited volume, mass and power are available for the ACS hardware. In the proposed ACS design for a 1U CubeSat, pointing is obtained through a two-stage approach: coarse and fine control modes. Fine control is achieved through the use of three reaction wheels or three magnetorquers and one reaction wheel along the pitch axis. Significant design work has been conducted to realize the proposed architecture. In this paper, we present (1) an overview of the proposed ACS design; (2) the verification results from the numerical simulation studies to demonstrate the performance of the proposed ACS design for a CubeSat-class nanosatellite; and (3) a series of air-bearing verification tests on nanosatellite ACS hardware that show some results of using the proposed nonlinear control design and compare performance with a PID controller.

Keywords: Attitude, Control, Magnetorquer, Reaction Wheel, CubeSat, Air Bearing.

---

*Corresponding author: Junquan Li, Ph.D, MITACS PDF fellow, Tel: +1 (416) 736-2100 ext. 22601, Dept. of Space Science and Engineering, York University, Canada.

1. Introduction

The development of nanosatellites (with a mass of 1-10 kg) is currently a significant trend in the area of space science and engineering research. The development of CubeSat-class nanosatellites started in 1999 as a collaborative effort between California Polytechnic State University and Stanford University, and has achieved great success as a way to efficiently construct and orbit small, inexpensive satellites using commercial technology. CubeSat, in general, is described as a class of nanosatellites ranging from 1 kg, 10 x 10 x 10 cm^3 and upwards in 10 cm increments of length. Currently more than 50 research groups around the world are developing CubeSat-class nanosatellites for technology demonstration, scientific and student training missions. A solid model of a typical 1U CubeSat (currently under development at York University, Canada) is shown in Figure 1.

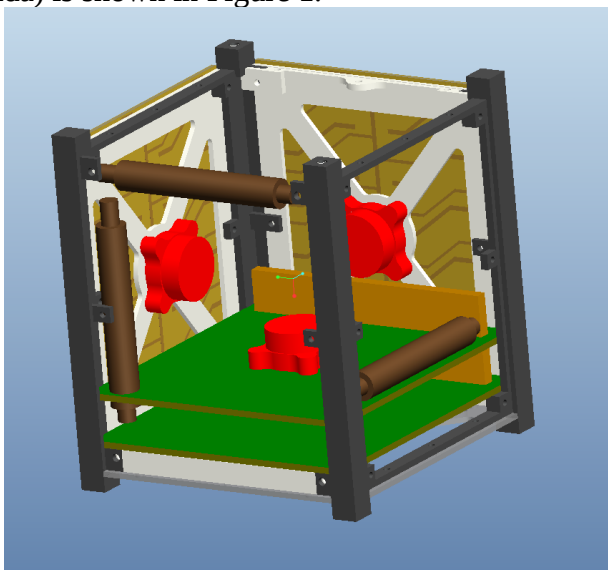

Figure 1: ACS in a CubeSat-class Nanosatellite (with Three Reaction Wheels & Three Magnetorquers)

Full-scale satellite attitude control systems are generally too large or too expensive to be installed in CubeSat-class nanosatellites [1], so passive attitude control systems have usually been used for nanosatellites in the past [2] [3]. More active attitude control subsystems [4] in

CubeSat-class nanosatellites have been implemented with the development of suitable actuators like magnetorquers (torque coils or torque rods) and small-sized reaction wheels [5] [6]. An overview of the proposed ACS design adopted for this study is shown in Figure 2. Currently, commercial nanosatellite torque rods and reaction wheels are too expensive for use in many research nanosatellite projects. The contributions of this research are the development of ACS hardware from off-the-shelf components, complete simulation of the ACS system, and validation testing of the ACS system for attitude control in the lab environment.

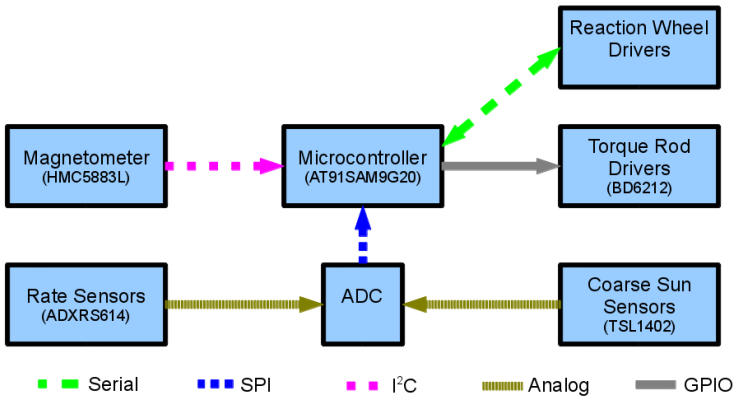

Figure 2: Overview of proposed ACS design for a CubeSat-class Nanosatellite

In this paper, we briefly describe ACS hardware proposed for CubeSat-class nanosatellite missions. We outline the hardware development of the ACS sensors and actuators in Section 2. In particular, we describe the sizing and design of the magnetorquers. More discussions on the ACS hardware selection, design and characterization for CubeSat-class nanosatellite missions, currently under development at York University can be also found in [7]-[11]. In Sections 3 and 4, we describe the satellite system models and the results from the simulation study based on the above ACS design. In section 5, we show the ground testing results of the hardware and software system, as well as some future work that is planned. Section 6 concludes the paper.

2. CubeSat ACS Hardware

2.1 Attitude Sensors

Attitude magnetic sensor hardware in the current study consists of a Honeywell HMC5883L three-axis MEMS magnetometer for magnetic field measurements. Angular rate information is obtained in three axes from three orthogonally-mounted Analog Devices ADXRS614 MEMS gyroscopes. The attitude control system is managed by an Atmel AT91SAM9260 32-bit ARM9 microcontroller that runs embedded Linux, with 32 MB SRAM, and 256 MB NAND Flash attached for volatile and non-volatile storage. All programming of control algorithms is accomplished in the C language using the GNU C compiler for the ARM processor. The system is designed for power-efficient operation because there is typically less than 3W generated from the photovoltaics on a typical 1U Cubesat in low-earth orbit, and a battery must be used during eclipse periods.

2.2 Magnetorquer Design

Magnetic torque coils, also referred to as magnetorquers, provide baseline control in many small satellites. They are commercially available in two typical configurations: in loose coils of flat-wound wire, and in tightly wound coils around a permalloy rod. The rod configuration is often preferred because of its compactness and rigidity, and the use of high-permeability materials for the core. To meet the mass and power requirements of a nanosatellite, a maximum weight of 30 g and a conservative maximum power draw of 0.2 W were set, and a typical maximum supply voltage between 3.7 V and 4.2 V were assumed to avoid having to step up voltage from a Li-Ion cell to supply actuator components.

Using the well-known solenoid equation and the relations derived in [13], a parametric analysis of the effect of core length and core radius on magnetic dipole moment was used to determine the optimal length and radius of the core material, given the wire thickness and

corresponding length to satisfy the power and dipole moment requirements. Figure 3 illustrates the effect of core sizing in metres on generated magnetic moment. The number of turns is implicitly determined, as the dipole moment of the torque rod is independent of the number of turns of wire, and the core radius is also constrained to sizes that are commercially available.

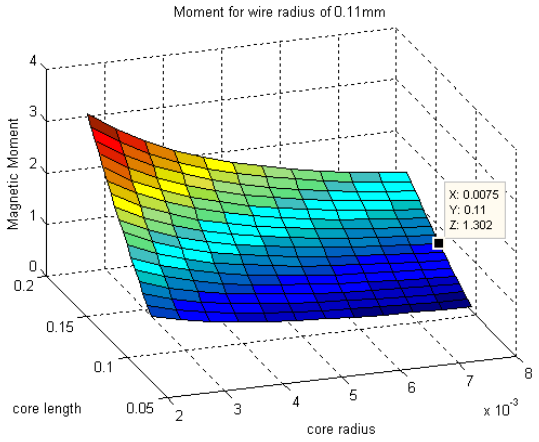

Figure 3 Magnetorquer Sizing Surface

To maximize the field generated with the dimensions while satisfying the design constraints, a prototype magnetorquer was designed with 70 mm long permalloy core, and 36 AWG wire to provide a maximum load power of 200 mW at 4.2 V. The design parameters of the constructed torque rods are shown in Table 1.

Table 1: Magnetorquer Parameters

Parameter	Value	Unit
Maximum Dipole Moment	0.37	A m^2
Total Mass	28	g
Number of Turns	6063	
Core Diameter	5.7	mm
Wire Diameter	0.127	mm
Wire Resistance	121	Ω
Maximum Current	34.7	mA

In order to precisely wind 36 AWG wires around a core, a coil winding machine was designed

and assembled using stepper motors and L298 H-bridge drivers controlled by an Atmel ATMega644P microcontroller. A permalloy core is rotated by one motor, while another positions a plastic feeder guide from the wire spool. The winder, shown with a completed torque rod in Figure 4, allows a torque rod to be automatically wound by setting the number of turns required, length of the core, and thickness of the wire, which determines the ratio of winding speed to feeder speed.

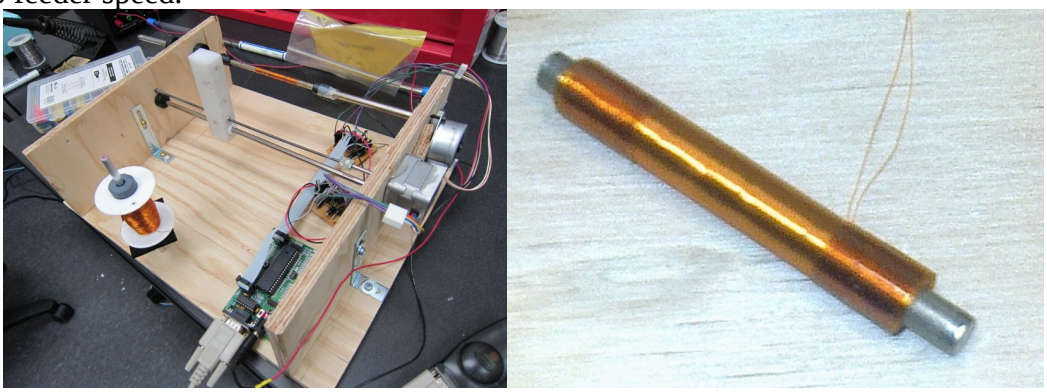

Figure 4 Magnetorquer Winding Apparatus and Completed Torque Rod

2.3 Reaction Wheel Design

Pointing and slew maneuvering of satellites is often accomplished by a reaction wheel or momentum wheel, which provide maneuvering torque and momentum storage [8]. Reaction wheels can provide a high degree of attitude control accuracy with the limitation that the wheel may reach saturation as its maximum speed is reached after continued use, requiring an additional momentum control method such as magnetorquers to desaturate the wheel in a process known as momentum dumping.

Each of the reaction wheels in the proposed ACS system consists of a machined steel cylinder that is press-fitted to the shaft of a Faulhaber brushless flat micro-motor. Design choices for the motor were limited to inexpensive commercial motors with low power consumption, and the reaction wheels were sized to provide maximum momentum storage given the mass and volume

constraints of a 1U CubeSat. Three reaction wheels can be used in the ACS if maximum control authority is required. Table 2 shows the design parameters of the reaction wheels used on the proposed ACS [16]. A completed reaction wheel assembly is shown in Figure 5.

Table 2: Reaction Wheel Parameters

Parameter	Value	Unit
Rotor Mass	0.214	kg
Moment of Inertia (axial)	9.41×10^{-5}	kg m^2
Moment of Inertia (transverse)	5.02×10^{-5}	kg m^2
Motor Shaft Torque	6.0×10^{-4}	N m
Maximum Speed	1539	rad/s
Supply Voltage	3.7-4.2	V

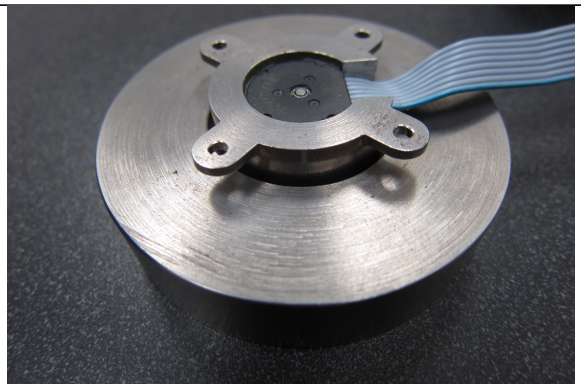

Figure 5: Reaction Wheel Assembly

2.4 Electronic Integration of ACS Components

To control the reaction wheel and magnetorquer hardware and house the attitude sensors and actuator drivers, a printed circuit board (PCB) was fabricated, shown in Figure 6. The board stacks with existing PC/104 sized on-board computer (OBC) hardware, and provides both I/O breakout and power supplies for the ACS hardware. It contains 3.3V and 5V switching supplies for the ACS sensors, as well as external interfaces for a battery and radio to be used specifically for air bearing ACS testing. The board makes a HMC5883 three-axis magnetometer, an ADXL345 3-axis accelerometer, and an ITG-3200 3-axis MEMS rate gyroscope available on the

OBC I^2C bus. Primary rate sensing for attitude control is accomplished by three independent ADXRS614 rate gyro units oriented on orthogonal axes by means of right-angle IC sockets and connected to the first three ADC channels on the OBC. This allows accurate high-speed sampling of rotation rates for use by the attitude controller. To drive the magnetorquers, three BD6212 integrated H-bridges are used, controlled by three PWM channels from the OBC and three general-purpose IO pins for current direction control. To allow one PWM signal and one direction pin to control each H-bridge, the inputs are demultiplexed by a SN74LVC1G8 tri-state output demultiplexer and pull-up resistors. In full operation, the board draws up to 100mW of power on average, though components can be shut down as needed to conserve power if not in use.

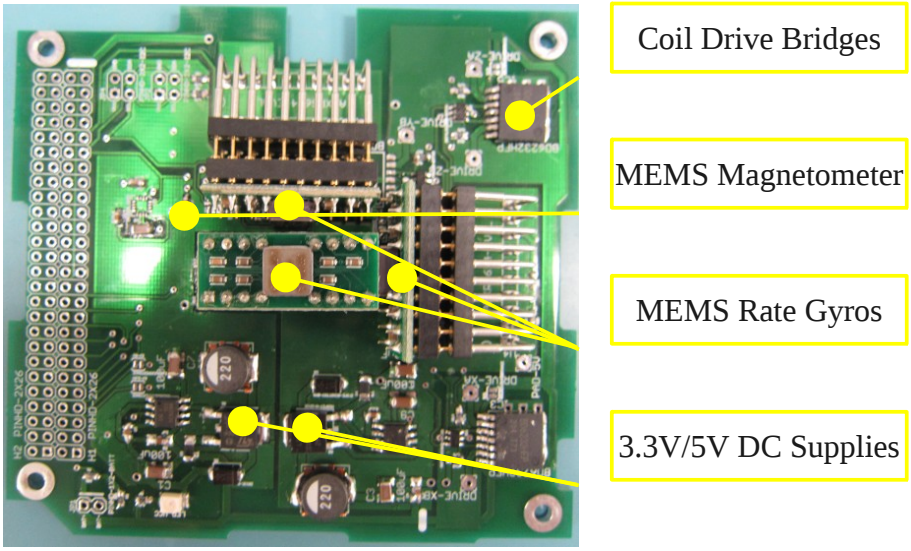

Figure 6 ACS Sensor and Actuator Board

3. System Models

3.1 Attitude Equations of Motions

The satellite is modelled as a rigid body with actuators that provide torques about three mutually perpendicular axes that define a body-fixed frame. The equations of motion [17] [20] are given by

$$\hat{J}\,\dot{\omega}_b = -\omega^{\times}\left(J_S\omega_b + A_i J_w \Omega\right) + A_i \tau_c + \tau_m + \tau_d \tag{1}$$

where $\omega_b = \left(\omega_{b1}\omega_{b2}\omega_{b3}\right)^T$ is the angular velocity of the satellite expressed in the body frame. J_s is the inertia matrix of the satellite. J_w is the inertia matrix of the reaction wheel, and $\hat{J} = J_s - A_i J_w A_i^T$. A_i is the layout matrix of the reaction wheels whose columns represent the influence of each wheel on the angular acceleration of the satellite. Ω is the velocity of the reaction wheel, τ_c is the torque control provided by the reaction wheel, τ_m is the torque control provided by the magnetorquers, and τ_d is the bounded external disturbance, which is a sum of the gravity gradient, aerodynamic, and solar radiation pressure disturbances.

3.2 Attitude Kinematics

The satellite attitude kinematics are represented using quaternions as shown in Eq. (2), where $q = (\bar{q}^T, q_4)^T = (q_1, q_2, q_3, q_4)^T$

$$\dot{q} = \frac{1}{2}\begin{pmatrix} q_4 I_{3\times 3} + \bar{q}^{\times} \\ -\bar{q}^T \end{pmatrix}\omega_b \equiv \frac{1}{2}A(q)\,\omega_b \tag{2}$$

In terms of Euler angles, we can also express the satellite attitude as

$$\begin{bmatrix} \dot{\psi} \\ \dot{\alpha} \\ \dot{\gamma} \end{bmatrix} = \begin{bmatrix} 1 & sin(\psi)tan(\alpha) & cos(\psi)tan(\alpha) \\ 0 & cos(\psi) & -sin(\psi) \\ 0 & sin(\psi/cos(\alpha)) & cos(\psi)/cos(\alpha) \end{bmatrix}\omega_b \tag{3}$$

where ψ is the roll angle about the x-axis, α is the pitch angle about the y-axis, and γ is the yaw about the z-axis.

3.3 Sensor Models

Magnetic field vectors are obtained in the orbit reference frame.

$$B_1 = \frac{M_e}{r_0^3}\left[cos(\omega_0 t)\left(cos(\epsilon)sin(i) - sin(\epsilon)cos(i)cos(\omega_e t)\right) - sin(\omega_0 t)sin(\epsilon)sin(\omega_e t)\right] \tag{4}$$

$$B_2 = \frac{-M_e}{r_0^3}\left[\left(cos(\epsilon)cos(i) + sin(\epsilon)sin(i)cos(\omega_e t)\right)\right] \quad (5)$$

$$B_3 = \frac{3M_e}{r_0^3}\left[sin(\omega_0 t)\left(cos(\epsilon)sin(i) - sin(\epsilon)cos(i)cos(\omega_e t)\right) - 2\,sin(\omega_0 t)sin(\epsilon)sin(\omega_e t)\right] \quad (6)$$

where ω_0 is the angular velocity of the orbit with respect to the inertial frame, r_0 is the distance from the center of the satellite to the center of the Earth, i is the orbital inclination, ε is the magnetic dipole tilt, ω_e Is the spin rate of the Earth, and M_e is the magnetic dipole moment of the Earth.

The magnetometer model for the sensed magnetic field is

$$H = C_k \begin{bmatrix} B_1 \\ B_2 \\ B_3 \end{bmatrix} + \eta_m + b_m \quad (7)$$

where C_k is the direction cosine matrix in terms of quaternions, η_m is the zero mean Gaussian white noise of the magnetometer, B is the vector formed with the components of the Earth's magnetic field in the body frame of the reference, as $B = C_k \begin{bmatrix} B_1 \\ B_2 \\ B_3 \end{bmatrix}$, and b_m is the magnetometer bias.

The angular velocity is measured from three rate gyroscopes. The model is given by

$$\omega_g = \omega + b_g + \eta_g \quad (8)$$

$$\dot{b}_g = -k_f * b_g + \eta_f \quad (9)$$

where ω_g is the output of a gyroscope, and ω is the real angular rate of the gyro. η_g and η_f are Gaussian white noise. b_g is the random drift of the gyro and k_f is the drift constant.

3.4 Actuator Models

Reaction wheels are widely used to perform precise satellite attitude maneuvers because they allow continuous and smooth control of internal torques. Torques are produced on the satellite by accelerating or decelerating the reaction wheels. Let the torque demanded by the satellite be denoted as τ_c , where $\tau_c = J_w(\dot{\Omega} + A_i \dot{\omega}_b)$. The input voltage e_a required to control the actuator dynamics of the reaction wheel can be written as

$$e_a = k_b \Omega - R_b k_t^{-1}(A_i \tau_c) \tag{10}$$

where k_t is the motor torque constant, k_b is the back-EMF constant, R_b is the armature resistance, and friction in the reaction wheels is ignored. The maximum voltage of the reaction wheel is 4.2 V and a dead-zone for the reaction wheel is estimated to be below 1 V. k_t Is 0.0082, k_b is 0.007, R_b is 0.5, and the moment of inertia of the reaction wheel is 0.0001 kg m^2.

4. Control Law Design and Simulation Results

4.1 Satellite Magnetic Attitude Control Laws

Magnetic control has been used over many years [24] [27] for small spacecraft attitude control. The main drawback of magnetic control is that magnetic torque is two dimensional and it is only present in the plane perpendicular to the magnetic field vector [25]. The accuracy of satellite attitude control systems using only magnetic actuators is known to be accurate on the order of 0.4-0.5 degrees [25]. The satellite can not be controlled precisely in three-dimensional space using only magnetorquers [25], but the combination of magnetorquers with one reaction wheel expands the two dimensional control torque possibilities to be three dimensional. The attitude accuracy of the combined actuators has been compared with three reaction wheel based attitude control in the references [25] [26]. Classical sliding mode control has also been used for magnetically actuated spacecraft [28] [29]. However, the proposed nonlinear adaptive fuzzy sliding mode control law has never been used in magnetic attitude control. This control law is

given by

$$\tau = -k_1 S - \theta^T \xi - k_2 \tanh\left(3K_u \varsigma S / \epsilon\right) \tag{11}$$

$$\dot{\theta} = \delta S \xi \theta \tag{12}$$

$$\tau_{ap} = \tau S / \|S^2\| S \tag{13}$$

$$M = \tau_{ap} \times B / \|B^2\| \tag{14}$$

Here, $\tau_m = M \times B$ where τ_m are the torques generated by the magnetorquers, M is the vector of magnetic dipoles for the three magnetorquers, and B is the vector formed with the components of the Earth's magnetic field in the body frame of the reference. S is the sliding surface. θ and ξ are the adaptive parameters and fuzzy weight functions generated by the fuzzy logic systems [22], and $\delta, k_1, k_2, K_u, \varsigma, \epsilon$ are positive constants used for tuning the control response.

Remark: AFSMC controller design details can be found in the author's previous papers [11]. The design includes: (1) sliding surface design [22]; and (2) fuzzy logic system design [22].

4.2 Simulation Results

The attitude detumbling and attitude stabilization phases are considered in this ACS simulation. The B-dot algorithm is used for the detumbling phase and the PD magnetic control law and adaptive fuzzy sliding mode magnetic control law are compared for the stabilization phase. We note that the orbit used for the present simulation study is a 500 km circular orbit with 45º inclination. At this altitude, the total disturbance torque for 1U CubeSats is estimated to be on the order of 5 x 10^{-7} Nm.

4.2.1 Detumbling Mode and Stabilization Mode

Scenario 1:

In the initial stage of ACS control, the angular velocities of the satellite are assumed to be all

0.169 rad/s as a result of separation from the launch vehicle. The ACS damps the angular rate by controlling three magnetorquers. The control logic generally used for detumbling is called B-dot control [1], as it makes use of the derivative of the magnetic field "B". For a CubeSat with moment of inertia J = *diag*(0.002,0.002,0.002) kgm^2, we include the external disturbances (aerodynamic, gravity gradient, solar pressure), set the desired quaternion to be (0,0,0,1), set the initial quaternion to be (0.1,-0.1,0.1,0.9849), and assume the magnetic dipole maximum of the rods to be 0.1 Am^2. The Euler angle tracking errors, angular velocity tracking errors, magnetic torque, and magnetic dipole results are shown in Figure 7. The satellite starts at the selected tip off rate and after 1 orbit, the angular velocities are reduced to the required rates before continuing with other ACS tasks.

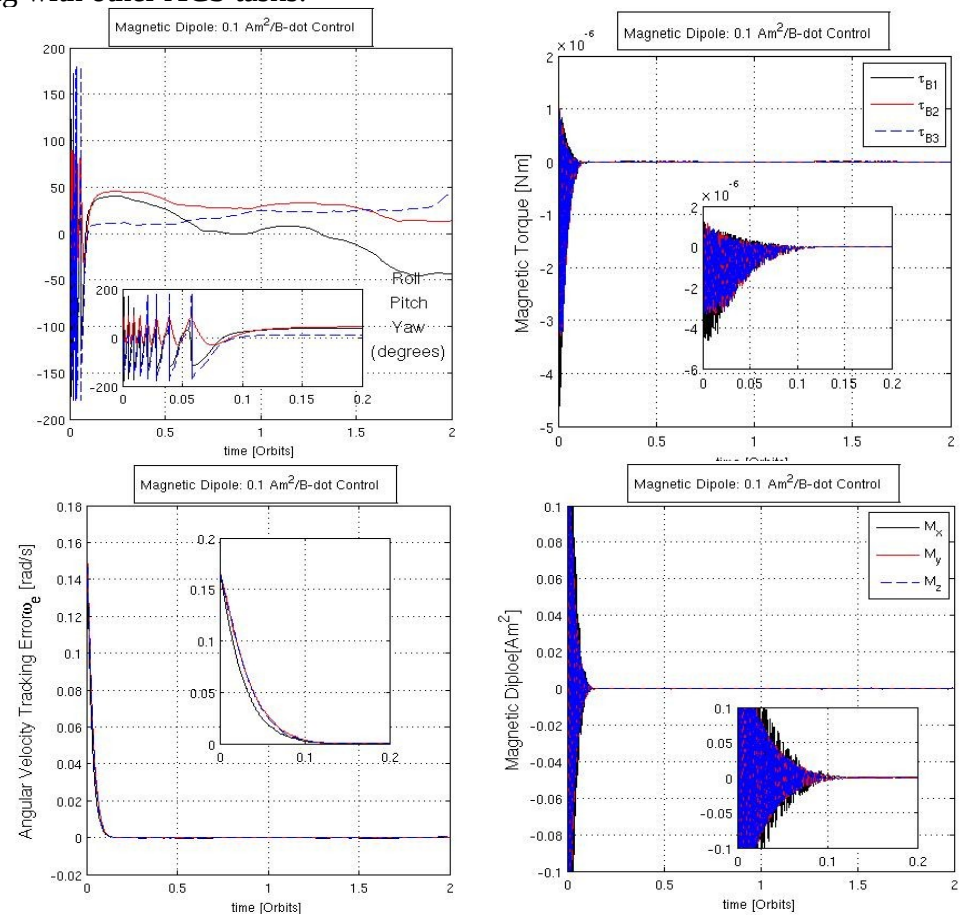

Figure 7: Detumbling Control Results

Scenario 2:

Now, we consider a CubeSat with the same moment of inertia and orbit, and assume the magnetic dipole maximum of the magnetorquer to be 0.4 Am^2 with a magnetometer sensor bias calculated by $20*10^{-4}*rand(1)$. Proportional-Derivative (PD) magnetic control [13] laws (shown in Eqs. (15)-(17)) are used in this simulation and the results over 6 orbits are shown in Figure 8. During the first three orbits, three magnetorquers are used for the detumbling mode. In the second three orbits, three magnetorquers and one reaction wheel are used for the stable mode. The attitude control error is less than 0.02 degrees while using the PD magnetic control laws.

$$\tau_m = M \times B \tag{15}$$

$$M = K_1 \omega_b \times B \tag{16}$$

$$M = K_1 \omega_b \times B + K_2 q \times B \tag{17}$$

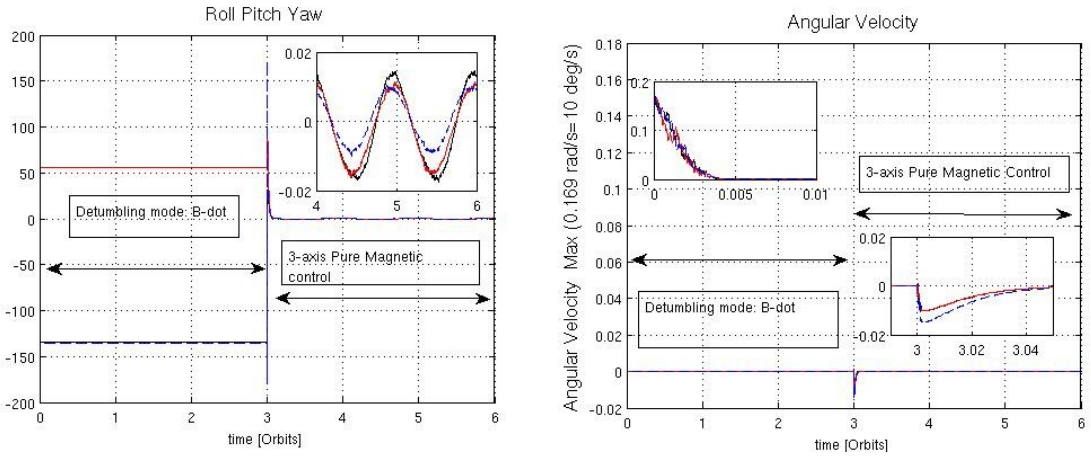

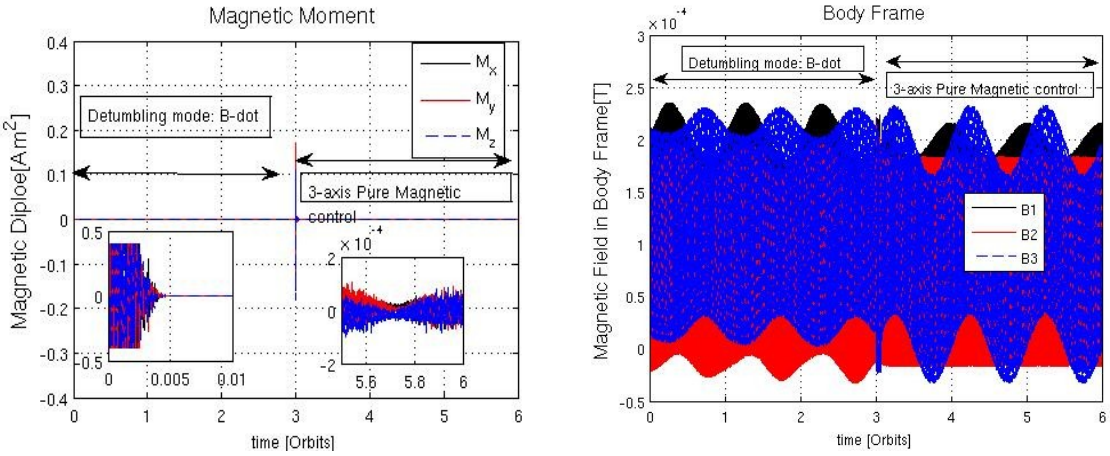

Figure 8: Detumbling Mode and Stable Mode Control Results

4.2.2 Attitude Stabilization Mode: Nadir and Limb Pointing with Three Magnetorquers and One Pitch Reaction Wheel.

Next, we consider the second stage of nanosatellite control with a low initial angular velocity after detumbling and large slew angle target for limb and nadir pointing. The configuration with three magnetorquers and one wheel [14] has been used for many years. In a real nanosatellite mission, hardware failures of the reaction wheels are very common [26]. When there are one or two wheel failures, the ACS can be switched from using three reaction wheels to three magnetorquers and one reaction wheel, and attitude control accuracy maintained using this method. The adaptive fuzzy sliding mode magnetic control laws are shown in Eqs. (11)-(14). The attitude control accuracy using the nonlinear adaptive fuzzy sliding mode control law is more robust to external disturbances than the PD magnetic control law in Eqs. (15)-(17).

Scenario 3:

An ACS using one reaction wheel and three magnetorquers as actuators for limb pointing with the desired quaternion set to (0,0.5736,0,0.8192) is examined using AFSMC over 10 orbits. The wheel dead zone is not considered here. The initial quaternion is (0.1,-0.1,0.1,0.9849) and initial angular velocity is (0.0169,0.0169,0.0169) rad/s. Considering only the pitch reaction wheel is available, the numerical simulations demonstrate that the proposed technique achieves a

high pointing accuracy (<0.09 degrees). The magnetic dipoles from the three magnetorquers, attitude tracking errors, wheel speed, and wheel voltage are shown in Figure 9.

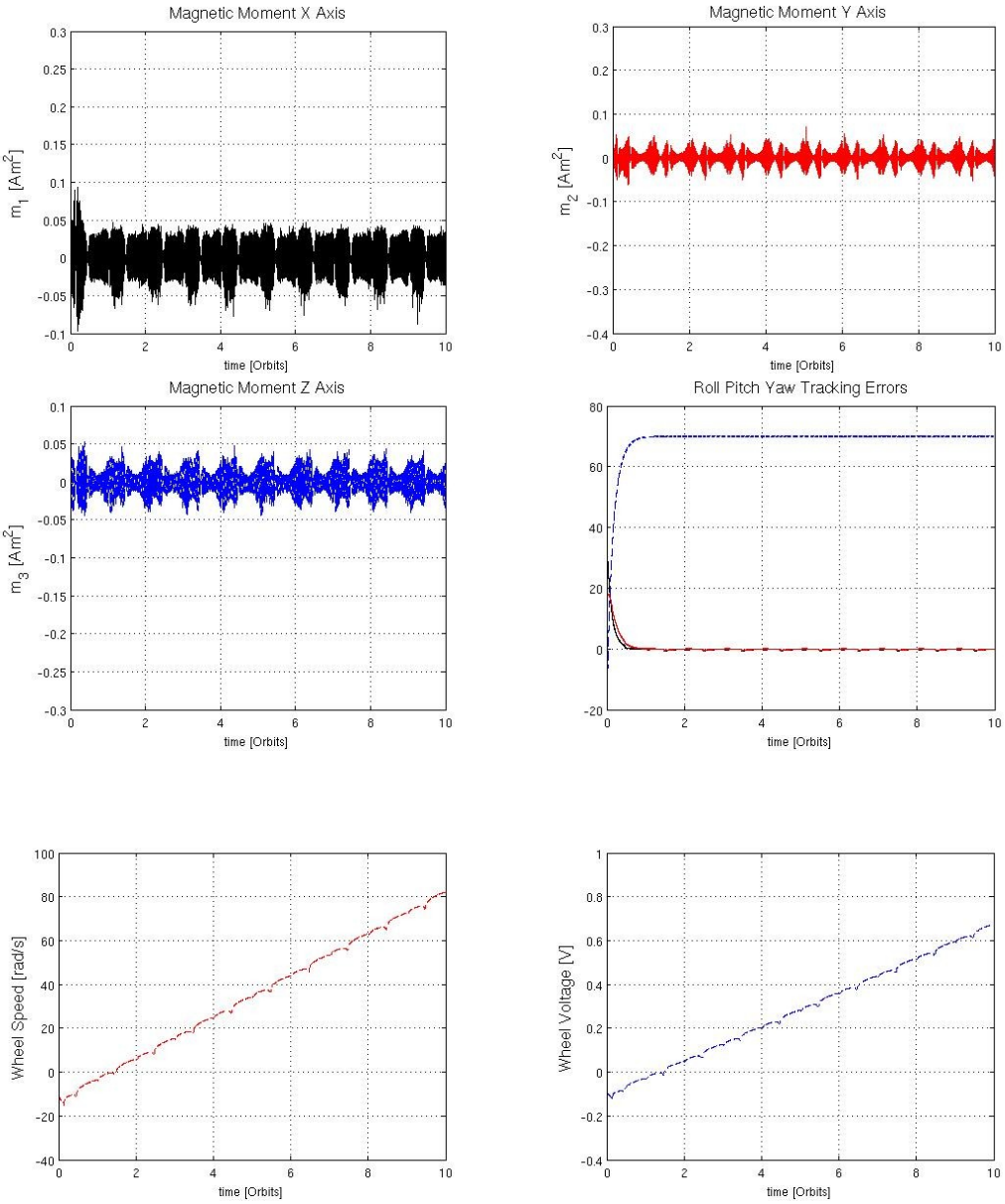

Figure 9: Limb Pointing Control Results using One Reaction Wheel and Three Magnetorquers

Scenario 4:

An ACS using one reaction wheel and three magnetorquers as actuators for nadir pointing with the desired quaternion set to (0,0,0,1) is examined using AFSMC over 10 orbits. The wheel dead zone is assumed to be +-1.0V. The initial quaternion is (0.1,-0.1,0.1,0.9849) and initial angular velocity is (0.0169,0.0169,0.0169) rad/s. The pitch reaction wheel and three magnetorquers are used. These simulations demonstrate that the proposed technique can also achieve high accuracy (<0.09 degrees with all disturbances) pointing control for small satellites. The magnetic dipoles of the three magnetorquers, attitude tracking errors, wheel speed, and wheel voltage are shown in Figure 10. It takes about 40 orbits for the wheel speed to increase from 0 to 2000 rpm (209 rad/s).

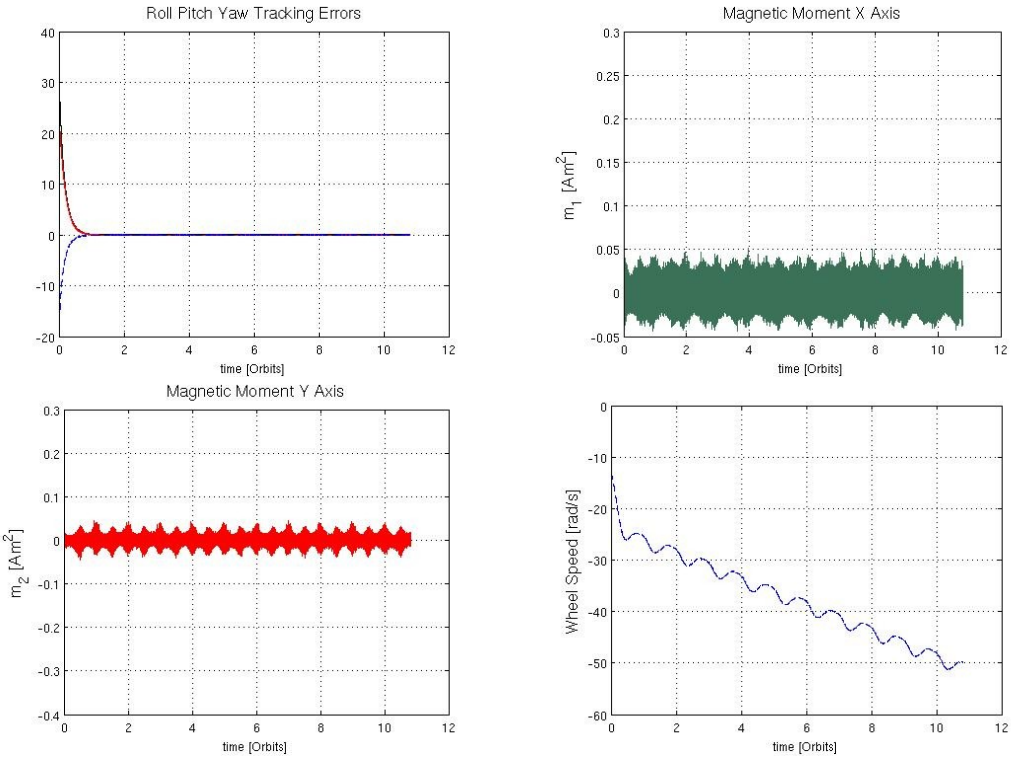

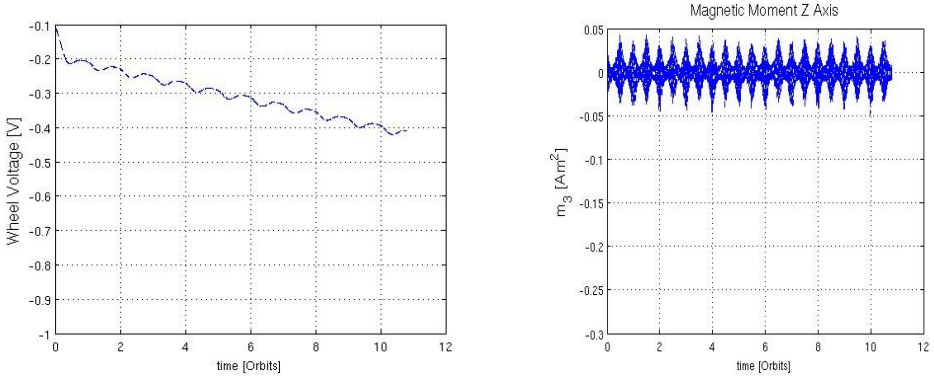

Figure 10: Nadir Pointing Control Results using One Reaction Wheel and Three Magnetorquers

4.2.3 Attitude Stabilization mode: Nadir Pointing with Three Reaction Wheels.

Scenario 5:

An ACS using three reaction wheels as actuators for nadir pointing with the desired quaternion set to (0,0,0,1) is examined using AFSMC over 0.1 orbits. The wheel dead zone is assumed to be +-1.0V. The initial quaternion is (0.1,-0.1,0.1,0.9849) and initial angular velocity is (0.0169,0.0169,0.0169) rad/s. This configuration can also achieve high attitude control accuracy (<0.008 degrees with all disturbances). The attitude control laws use Eqs. (11)-(12). The settling time is shorter and the pointing accuracy higher than that achieved using only three magnetorquers and one reaction wheel as actuators. However, the power consumption is higher than using three magnetorquers and one reaction wheel. The Euler angle tracking errors, control inputs, wheel speeds, and wheel voltages are shown in Figures 11-14.

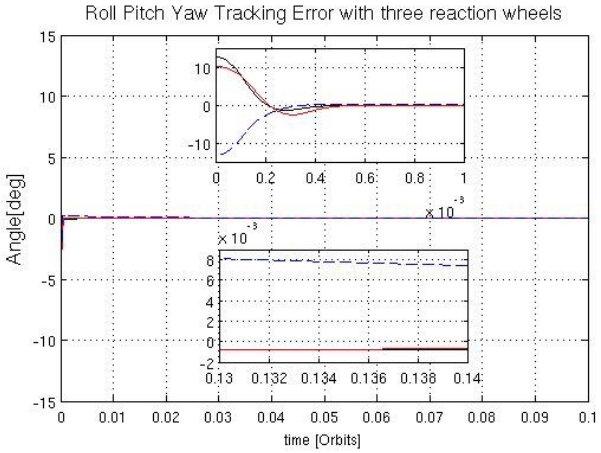

Figure 11: Nadir Pointing Control Results using Three Wheels: Euler Angle Tracking Errors

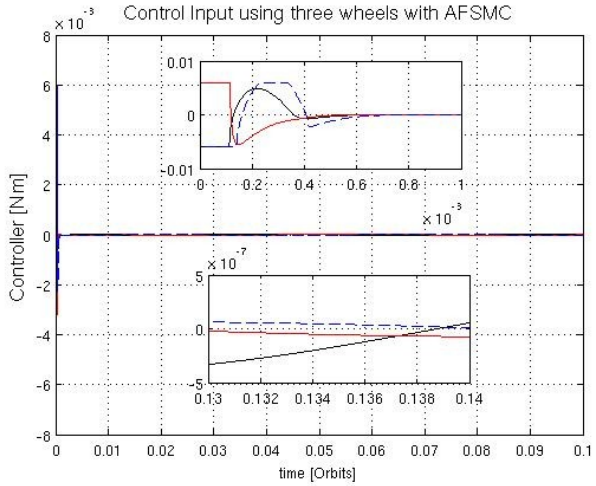

Figure 12: Nadir Pointing Control Results using Three Wheels: Control Input

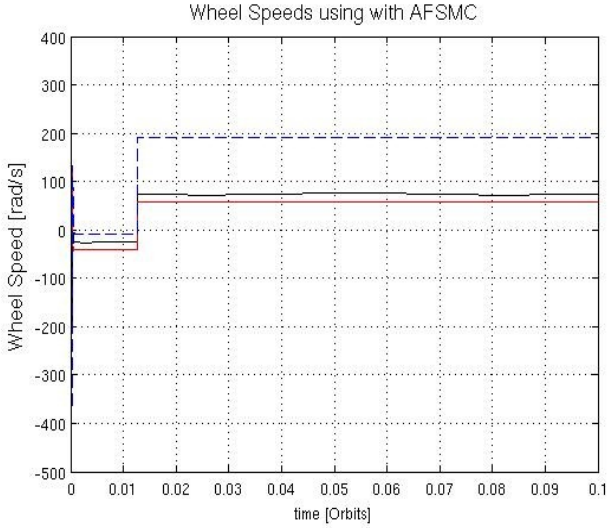

Figure 13: Nadir Pointing Control Results using Three Wheels: Wheel Speed

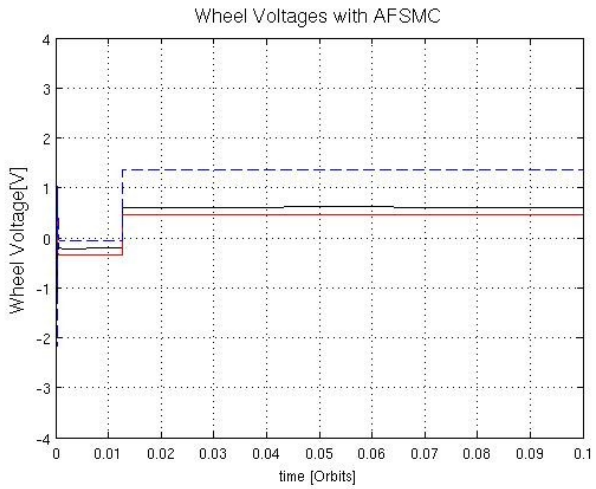

Figure 14: Nadir Pointing Control Results using Three Wheels: Wheel Voltage

5. Satellite Attitude Control System Hardware Testing

5.1 Spherical Air-bearing Test-Bed for Satellite Attitude Control Systems

The ground testing of the proposed CubeSat ACS design was performed at York University using a nanosatellite attitude control testbed. This facility consists of a spherical air bearing platform [15] [23] suspended upon a thin layer of air that provides three degrees of rotational freedom with negligible friction for ACS testing. The platform consists of a manual balancing system and electronics that include the on-board computer (OBC), a wireless transceiver for telemetry, a reference inertial measurement unit (IMU), a power distribution board, and Li-Ion batteries. The air bearing system configured for 1U CubeSat testing is shown in Figure 15.

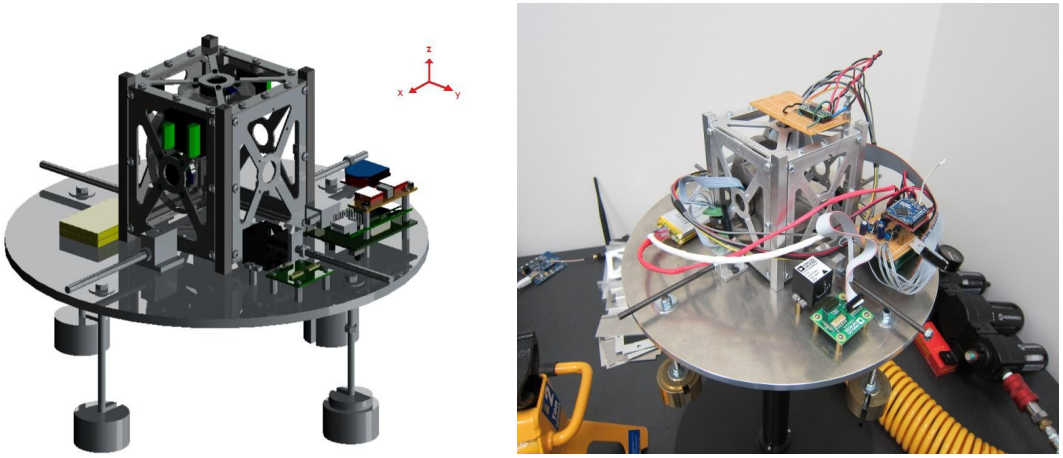

Figure 15: Air Bearing ACS Ground Testing System

5.2 Ground Test Results: ACS Testing Results with Three Reaction Wheels Actuators

Nonlinear attitude control has been explored widely in theory [17] [18] [19]. In real satellite applications, nonlinear controllers are usually not selected due to their complexity of design. We have tested similar nonlinear control algorithms [11] on this spherical air bearing system. We now test the proposed control method (from Eqs. (11)-(12)) on this system using the sensors and ACS board described above and three-axis reaction wheel actuation. A PID control law is also used for comparison on the same hardware. The control laws are programmed in the C language, and the OBC runs the Linux operating system. More details of the implementation can be also found in [11]. The control law design parameters used are given in Tables 3 and 4.

Table 3: PID Controller Parameters for Air Bearing Testing

Name	Values
Proportional Parameters	0.03
Integral Parameters	0.0001
Derivative Parameters	0.11

Table 4: AFSMC Controller Parameters for Air Bearing Testing

Name	Values
Sliding Surface Gain	0.00001, 100
Fuzzy Membership Function	1, 1
Adaptive Gains $\delta, K_u, \varsigma, \epsilon$	0.1, 0.36, 0.01, 2
AFSMC Parameter k_1	0.004
AFSMC Parameter k_2	0.0025

Figures 16 and 17 show the attitude tracking errors, AFSMC/PID control output signals, reaction wheel voltages, and reaction wheel velocities for a 90 degree yaw slew of the system about the z-axis while maintaining 0 degrees of roll and pitch. Due to the difficulty of perfectly balancing the air bearing system, a gravitational disturbance, larger than normal in size, is considered to be present about the x and y rotational axes. Compared to the PID controller, the AFSMC controller uses nearly the same gain and has much better tracking performance under these conditions.

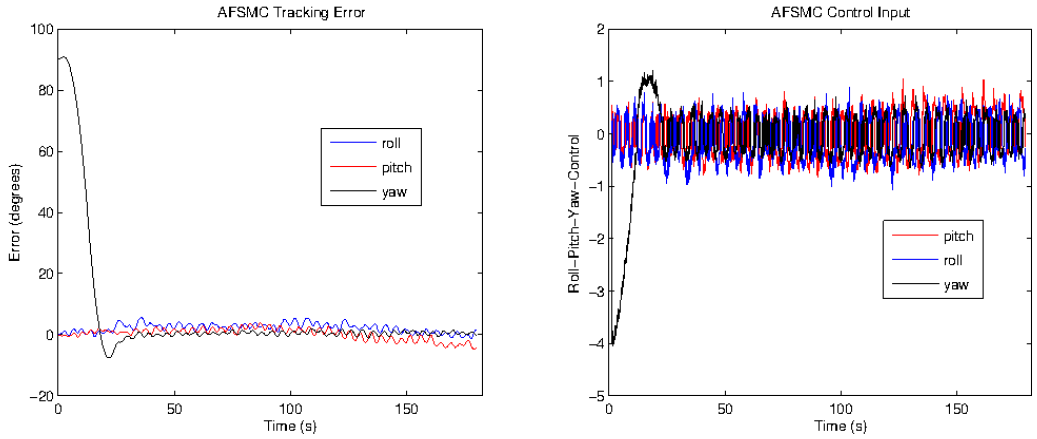

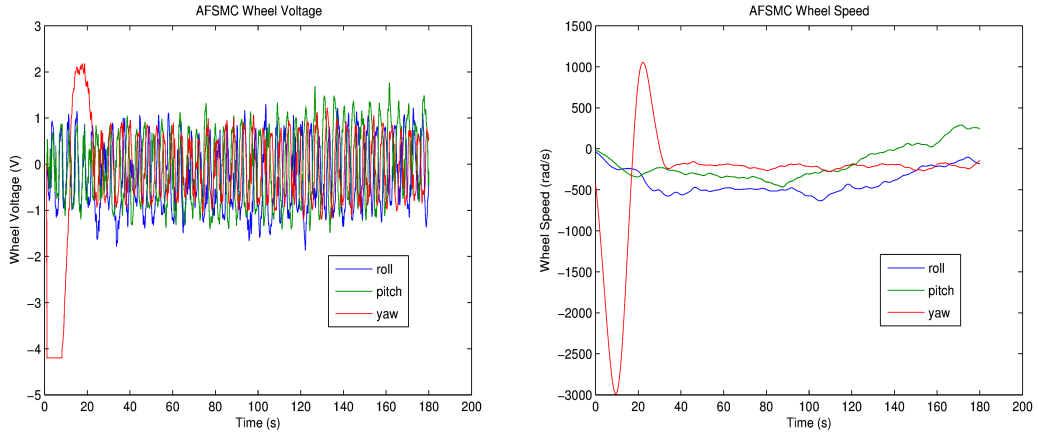

Figure 16: Air Bearing Nonlinear AFSMC Controller Results

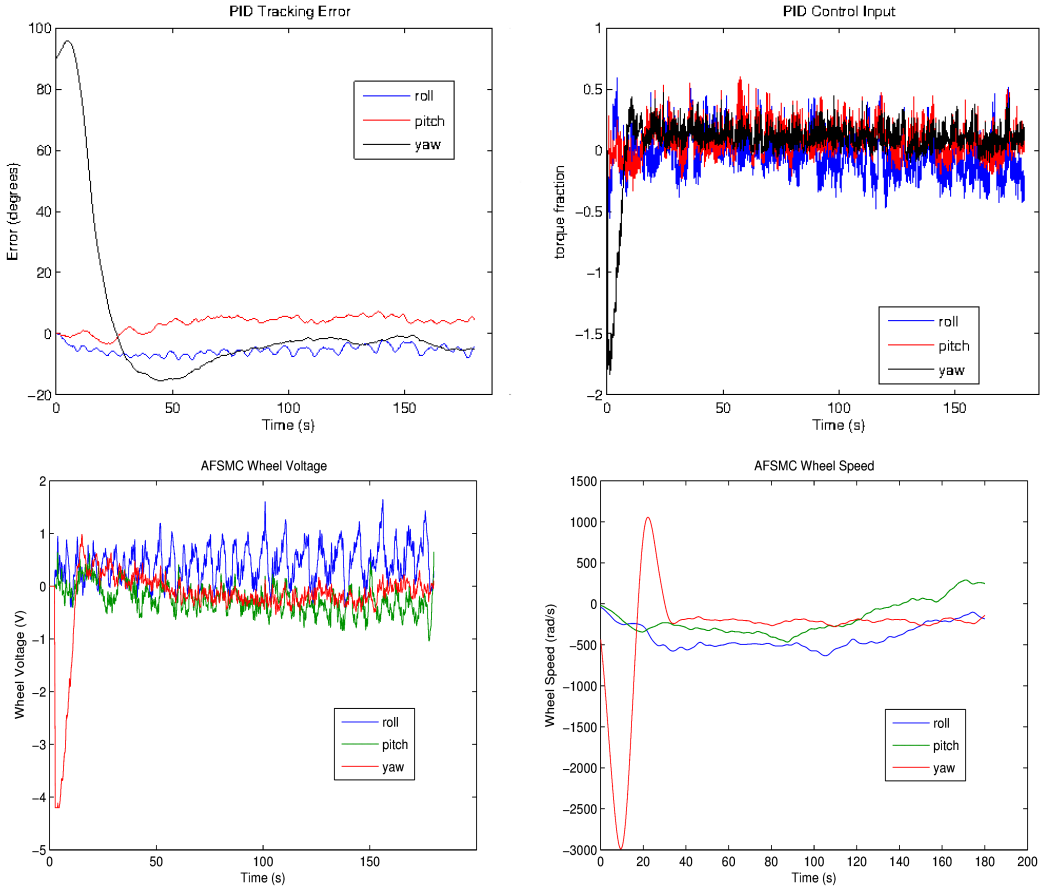

Figure 17 Air Bearing Nonlinear PID Controller Results

5.3 Future Work

While this ground test demonstrates the effectiveness of the proposed ACS design, it is difficult to test the performance of pure and hybrid magnetic control methods as the Earth's magnetic field present in the test facility is constant with many sources of additional magnetic noise. As the next step in developing the ACS test facility, a Helmholtz cage for magnetic control tests has been designed and fabricated. The magnetic cage and the air bearing system in the lab are shown in Figure 18, and are presently being prepared for air bearing magnetic control. Future work will demonstrate the effectiveness of magnetic control in further ground testing.

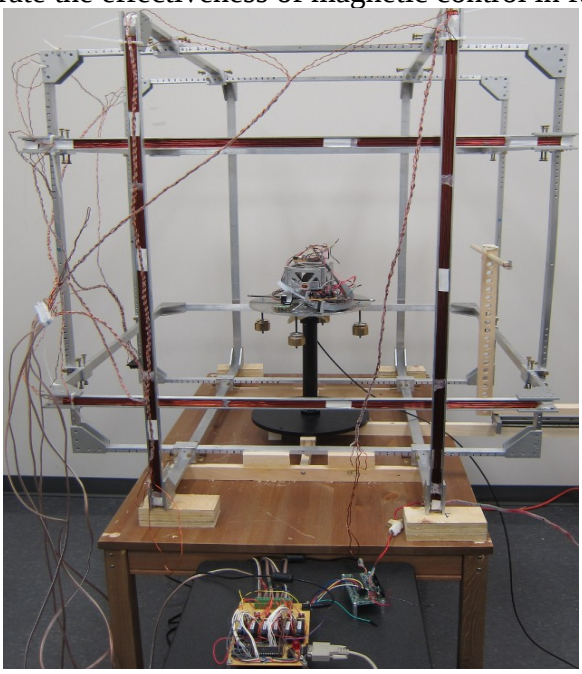

Figure 18: Helmholtz Cage for Magnetic Field Generation

6. Conclusion

In this paper, the proposed ACS uses three reaction wheels as actuators or one wheel with three magnetorquers as actuators. The hardware designs used in the ACS are also described for prototype development. In this research, nonlinear adaptive fuzzy sliding mode controllers

(AFSMC) are used for numerical simulations and air bearing testing. Five different scenarios of numerical simulation results for 1U CubeSat-class nanosatellite show the effectiveness of the proposed ACS design for detumbling and attitude pointing purposes. The 1U CubeSat-class nanosatellite attitude control test results on the air bearing system provide a promising comparison of the AFSMC controller with a conventional PID controller. The Helmholtz cage that is now available for use with the air bearing system will continue to provide further results to support the proposed ACS design. This approach will allow an inexpensive and capable nanosatellite ACS system to be developed for academic use. The 1U CubeSat-class nanosatellite testing hardware can be also extended for 2U or 3U CubeSat-class nanosatellite research in the future.

Acknowledgments

The authors gratefully acknowledge the support provided by COM DEV Ltd., NSERC, MITACS and OCE. The authors would also like to acknowledge the work of M. Cannata, I. Proper and T. Ustrzycki, G. Benari, and H. Hakima in this paper.

References

[1] Y. W. Jan, J. C. Chiou, Attitude Control System for ROCSAT-3: Microsatellite: a Conceptual Design, Acta Astronautica, 56 (2005) 439 – 452.

[2] M. Ovchinnikov, V. Pen'kov, O. Norberg, S. Barabash, Attitude Control System for the First Swedish Nanosatellite “MUNIN”, Acta Astronautica, 46 (2-5) (2000) 319-326.

[3] M. I. Martinellia, R. S. S. Peña, Passive 3 Axis Attitude Control of MSU-1 Pico-satellite, Acta Astronautica, 56 (2005) 507-517.

[4] G. P. Candini, F. Piergentili, and F. Santoni, Miniaturized Attitude Control System for Nanosatellites, Acta Astronautica, 81 (2012) 325-334.

[5] T. Xiang, T. Meng, H. Wang, K. Han, Z.-H. Jin, Design and On-Orbit Performance of the Attitude Determination and Control System for the ZDPS-1A Pico-satellite, Acta Astronautica, 77 (2012) 182-196.

[6] M. Abdekrahman, S. Y. Park, Integrated Attitude Determination and Control System via Magnetic Measurements and Actuation, Acta Astronautica, 69 (2011) 168-185.

[7] M. Cannata, Development of a Sun Vector Determination Algorithm for Cubesat-Class Spacecraft, M.Sc. Thesis, Dept. of Earth and Space Science and Engineering, York University, Toronto, Canada, August 2010.

[8] I. Proper, Reaction Wheel Design, Construction and Qualification Testing, M.Sc. Thesis, Dept. of Earth and Space Science and Engineering, York University, Toronto, Canada, August 2010.

[9] J. Li, M. A. Post, R. Lee, Real Time Fault Tolerant Nonlinear Attitude Control System for Nanosatellite Application, AIAA Infotech@Aerospace 2012 Conference, June. 19-21, Garden Grove, California, 2012.

[10] J. Li, M. A. Post, R. Lee, Nanosatellite Air Bearing Tests of Fault-Tolerant Sliding-Mode Attitude Control with Unscented Kalman Filter, AIAA Guidance, Navigation, and Control Conference, August. 13-16, Minneapolis, Minnesota, 2012.

[11] J. Li, M. A. Post, R. Lee, Nanosatellite Attitude Air Bearing System using Variable Structure Control, IEEE 25th Annual Canadian Conference on Electrical and Computer Engineering, April. 29- May. 2, Montreal, Canada, 2012.

[12] M. F. Mehrjardi, M Mirshams, Design and Manufacturing of a Research Magnetic Torquer Rod, Contemporary Engineering Sciences, 3 (5) (2010) 227-236.

[13] D. V. Guerrant, Design and Analysis of Fully Magnetic Control for Picosatellite Stabilization, M.Sc. Thesis, California Polytechnic State University, 2005.

[14] M. Chen, S. J. Zhang, F. H. Liu, and Y. C. Zhang, Combined attitude control of small satellite using one flywheel and magnetic torquers, in Proceeding of 2nd International *Symposium* Systems and Control in Aerospace and Astronautics, December 10-12, Shenzhen, China, 2008.

[15] J. Prado, G. Bisiacchi, L. Reyes, E. Vicente, F. Contreras, M. Mesinas, A. Juárez, Three-Axis Air-Bearing Based Platform for Small Satellite Attitude Determination and Control Simulation, Journal of Applied Research and Technology, 3 (3) (2005) 222-237.

[16] T. Ustrzycki, Spherical Air Bearing Testbed for Nanosatellite Attitude Control Development. M.Sc. Thesis, Dept. of Earth and Space Science and Engineering, York University, Toronto, Canada, August, 2011.

[17] C.-H . Won, Comparative Study of Various Control Methods for Attitude Control of a LEO Satellite, Aerospace Science and Technology, 5 (1999) 323–333.

[18] K.-S. Kim, K. D. Kim, Robust Backstepping Control for Slew Maneuver using Nonlinear Tracking Function, IEEE Transactions on Control Systems Technology, 11 (6) (2003) 822–829.

[19] S. C. Lo, Y. P. Chen, Smooth Sliding Mode Control for Spacecraft Attitude Tracking Maneuvers, Journal of Guidance Control and Dynamics, 18 (6) (1995) 1345–1349.

[20] J. Y. Lin, S. Ko, C.-K. Ryoo, Fault Tolerant Control of Satellites with Four Reaction

Wheels, Control Engineering Practice, 16 (2008) 1250–1258.

[21] S. Janardhanan, M. U. Nabi, P. M. Tiwari, Attitude Control of Magnetic Actuated Spacecraft using Super-Twisting Algorithm with Nonlinear Sliding Surface, 12 th IEEE Workshop on Variable Structure Systems, VSS 12, January 12-14, Mumbai, 2012,

[22] J. Li, K. D. Kumar, Fault Tolerant Attitude Synchronization Control during Formation Flying, Journal of Aerospace Engineering, 24 (3) (2011) 251-263.

[23] J. J. Kim, B. N. Agrawal, Automatic Mass Balancing of Air-Bearing-Based Three-Axis Rotational Spacecraft Simulator, AIAA Journal of Guidance, Control, and Dynamics, 32 (3) (2009) 1005-1017.

[24] E. Silani, M. Lovera, Magnetic Spacecraft Attitude Control: a Survey and Some New Results, Control Engineering Practice, 15 (2005) 357-371.

[25] Z. Q. Zhou, Spacecraft Attitude Tracking and Maneuver using Combined Magnetic Actuators, AIAA Guidance, Navigation, and Control Conference 2010, August 2-5, Toronto, Ontario, Canada, 2010.

[26] J. R. Forbes, C. J. Damaren, Geometric Approach to Spacecraft Attitude Control using Magnetic and Mechanical Actuation, AIAA Journal of Guidance, Control, and Dynamics, 33 (2) (2010) 590-595.

[27] C. J. Dameran, Hybrid Magnetic Attitude Control Gain Selection, Proc. ImechE, Part G: Journal of Aerospace Engineering, 23 (2009) 1041-1047.

[28] R. Wisniewski, Satellite Attitude Control using magnetic Actuation Only, Ph.D. Dissertation, Dept. of Control Engineering, Aalborg University, Denmark, 1996.

[29] P. Wang, Y. B. Shtessel, Y. Wang, Y, Satellite Attitude Control using only

magnetorquers, Proceeding of Thirtieth Southeastern Symposium on System Theory, March 8-10, West Virginia University, Morgantown, West Virginia, 1998.